A statistical comparison of solar wind propagation delays derived from multispacecraft techniques

N. A. Case[1] and J. A. Wild[1]

Received 21 June 2011; revised 14 November 2011; accepted 28 November 2011; published 9 February 2012.

[1] We present a large-scale statistical study of the solar wind propagation delay between NASA's Advanced Composition Explorer spacecraft and ESA's Cluster 1 spacecraft. This study focuses on those periods when Cluster was within the unimpeded solar wind, upstream of the bow shock nose, between 2001 and 2010. Using a cross-correlation method to compare the ACE and Cluster data, nearly 5000 propagation delays have been calculated and compared to both corresponding propagation delays in the OMNIweb data set and to those computed by a simple "flat" (i.e. distance/speed) propagation model. The results show that statistically there is little difference between the OMNI and flat propagation delay times and that the cross-correlation method agrees well with both, but there are times when the various methods give significantly different propagation estimates. There is found to be no influence on the relationship between the estimated and observed solar wind propagation delays from the solar wind speed or IMF orientation.

Citation: Case, N. A., and J. A. Wild (2012), A statistical comparison of solar wind propagation delays derived from multispacecraft techniques, *J. Geophys. Res.*, *117*, A02101, doi:10.1029/2011JA016946.

1. Introduction

[2] To understand many of the processes in the coupled solar wind-magnetosphere-ionosphere system, it is necessary to characterize the interplanetary conditions which drive them. Many magnetospheric phenomena, such as geomagnetic storms and auroral substorms, are known to be driven by the solar wind with key aspects of their evolution tied to particular solar wind and interplanetary magnetic field (IMF) conditions. To correctly attribute the sequence of cause and effect between magnetospheric dynamics and drivers in the solar wind and embedded IMF, accurate specification of interplanetary conditions is essential.

[3] Although many satellites sample the solar wind and IMF upstream of the Earth, continuous monitoring of the field and plasma conditions impinging upon the magnetosphere some 10 R_E sunward of the planet is not possible due to the orbital motion of the satellites. A common approach is to exploit satellite measurements made at a location much further upstream and apply a temporal delay to account for the propagation of solar wind and IMF structures from the satellite to the magnetosphere, assuming that the structures do not evolve in the intervening period. The Advanced Composition Explorer (ACE) satellite is particularly suited to this role. ACE orbits about Lagrangian liberation point 1 (L1) and is, therefore, constantly within the antisunward flowing solar wind ~240 R_E (~1.5 million km) upstream of Earth [*Stone et al.*, 1998].

[4] Previous studies have shown that most propagation delays are of the order of 1 hour [*Mailyan et al.*, 2008], although it is not accurate to assume this value for all intervals. Variations of ±30 min in the delay times, even over short timescales, are possible [*Weimer et al.*, 2003].

[5] Several studies have set out to ascertain more accurate values for the solar wind propagation delay under various conditions [e.g., *Horbury et al.*, 2001; *Weimer et al.*, 2003; *Weimer and King*, 2008]. However, no method has been proposed that is able to accurately determine a delay for all situations. Indeed, most methods outlined are applied to the solar wind during certain conditions, primarily when there is a discrete discontinuity in the IMF [e.g., *Mailyan et al.*, 2008].

[6] The difficulty in accurately predicting the delay time of the solar wind has been the primary reason for the development of OMNIWeb (http://omniweb.gsfc.nasa.gov). OMNIWeb combines data from multiple spacecraft (ACE, Wind, IMP 8 and Geotail) to produce a high resolution database of solar wind conditions lagged to the nose of the Earth's bow shock. They calculate the appropriate lag time to apply to the data, using the time-shift equation given in equation (1):

$$\Delta t = \frac{n \cdot (R_d - R_o)}{n \cdot V} \tag{1}$$

where R_o represents the location of an observing spacecraft (i.e. ACE) and R_d represents the displaced location (i.e. the bow shock nose). The solar wind velocity is denoted as V and the phase front normal (PFN) of the solar wind is n.

[7] The determination of the PFN, using a single spacecraft observer, is non-trivial and is estimated using a suite of methods based upon Minimum Variance Analysis (MVA) and Cross Product (CP) methods. The OMNI website notes, however, that when applied to the whole data set all the methods give statistically the same results.

[1]Department of Physics, Lancaster University, Lancaster, UK.

0148-0227/12/2011JA016946

[8] Although not routinely available, the disposition of magnetospheric spacecraft, such as Cluster, leads to intervals when a satellite is located in the solar wind, just upstream of the bow shock, for a short period (typically a few hours). Such conjunctions of satellites, one in the vicinity of the L1 point and another just upstream of the bow shock, present opportunities to compare the estimated interplanetary conditions impinging upon the magnetosphere (based upon lagged upstream data) to in situ solar wind and IMF measurements. These well-instrumented periods therefore allow the accuracy of the solar wind propagation techniques to be examined. In this study we present solar wind propagation delays, as calculated by a cross-correlation method using L1 and near-Earth satellites, and compare these to the corresponding propagation delays computed by the popular OMNIWeb tool and simple flat propagation estimates.

2. Methodology

[9] Simultaneous data were obtained from both the ACE and the Cluster 1 satellites during periods where Cluster's orbit would place it, for the most-part, sunward of the Earth's magnetosphere. This condition restricted our study to the months of January to April, from years 2001 to 2010, inclusive.

[10] Two further restrictions were imposed, whereby only data recorded when Cluster was located at distances greater than 15 R_E upstream of Earth and when the ion temperature, as measured by the Cluster Ion Spectrometer (CIS), was less than 1 keV, to ensure that Cluster was outside of the bow shock, was used. This allows for direct comparison with OMNI data which has been propagated from an upstream spacecraft to the bow shock nose, as determined by the bow shock model of *Farris and Russell* [1994] and the magnetopause model of *Shue et al.* [1997].

[11] Since Cluster was not necessarily located at the bow shock when the data was recorded, the delay time calculated may not represent the true delay time for propagation to the bow shock. The delay calculated was therefore increased by an appropriate factor based upon Cluster's location and the location of the bow shock, as given by OMNI, at that time.

[12] By performing a cross-correlation analysis on the clock angles of these two sets of data, it is possible to determine an appropriate delay between the time series of IMF measurements at ACE and the equivalent time series occurring some time later at Cluster (assuming both time series are measurements of the same IMF variations but displaced in time).

[13] The clock angle was chosen to perform the correlation on since it gives an overview measure of the IMF, rather than a singular component of the IMF (e.g. B_z), and since it yielded a greater number of delays than the field magnitude.

[14] The IMF clock angle is calculated by taking the arctangent of the y-component of the magnetic field over the z-component, as shown in equation (2). It describes the direction of the IMF in the y/z plane.

$$\theta = \arctan\left[\frac{By}{Bz}\right] \tag{2}$$

[15] This cross-correlation analysis can be repeated for all times when both ACE and Cluster data are available, yielding a database of ACE-to-Cluster propagation delays. These delays can then be directly compared to any other method or model that estimates the propagation delay of the solar wind from ACE. In this study, the delays derived from the cross-correlation analysis are directly compared to contemporaneous delays within the OMNI data set and to a simple antisunward planar propagation delay model, known as a "flat" delay.

[16] The flat delay assumes that the solar wind simply traverses from point A, i.e. ACE, to point B, i.e. the bow shock nose, at a constant speed and that there are no fundamental changes to the solar wind as it traverses. Since OMNI calculates the lag time to the bow shock nose, and since the nose is not fixed in position, the distance the solar wind travels is variable and is dependent upon the model used. The position of the bow shock nose, in the flat propagation calculation, is taken to be the same as OMNI predicts, so as to eliminate any differences due to modeling. The position of ACE also varies slightly due to its orbital configuration at L1 which is taken into account. Since this is a simple propagation calculation, only the separation distance and propagation velocity in the GSE x-direction are used in the computation. The GSE x-component of the solar wind velocity is taken as it passes ACE and is assumed to be constant throughout its Earthward propagation.

[17] As shown in equation (3), the delay is calculated by dividing the separation distance of ACE and the bow shock nose, in the GSE x-direction, (Δs_x), by the average x-component of the solar wind velocity, measured by ACE, during the 10 min correlation period (V_{avg}).

$$t_{lag} = \frac{\Delta s_x}{V_{avg}} \tag{3}$$

2.1. Correlation Conditions

[18] Performing a cross-correlation analysis of two data sets is most straight forward when the data are joined to the same time tags, however, the three different data sources used in this study provide data at different cadence. The data are therefore re-sampled to the required cadence using a mean average over the resample period, ignoring any bad data flags.

[19] The length of the period over which the cross-correlation analysis is performed can be important and must first be defined. Too short a period may result in no correlation being obtained while too long a period may be affected by any long term repeating structures. After reviewing several different periods and the resulting correlation profiles on the same sets of data, a period of approximately 10 min, or exactly 38 $\times$ 16 second resolution data points, was generally found to provide the highest correlation coefficient. Once the maximum cross-correlation coefficient for the two 38 point time series has been computed, both of the raw time series are shifted by 1 min, a new 38 point time series extracted and the cross-correlation coefficient re-computed. A period of 1 min for the shifting was chosen to produce a data set of the same cadence as the OMNI data set.

[20] Determining the limits of the cross-correlation analysis, i.e. the minimum and maximum lags over which to perform the comparison, is non-trivial and, for best results, would require a priori knowledge of the propagation delay time. However, it is clear that there must be some propagation delay between ACE and Cluster, since the solar wind travels

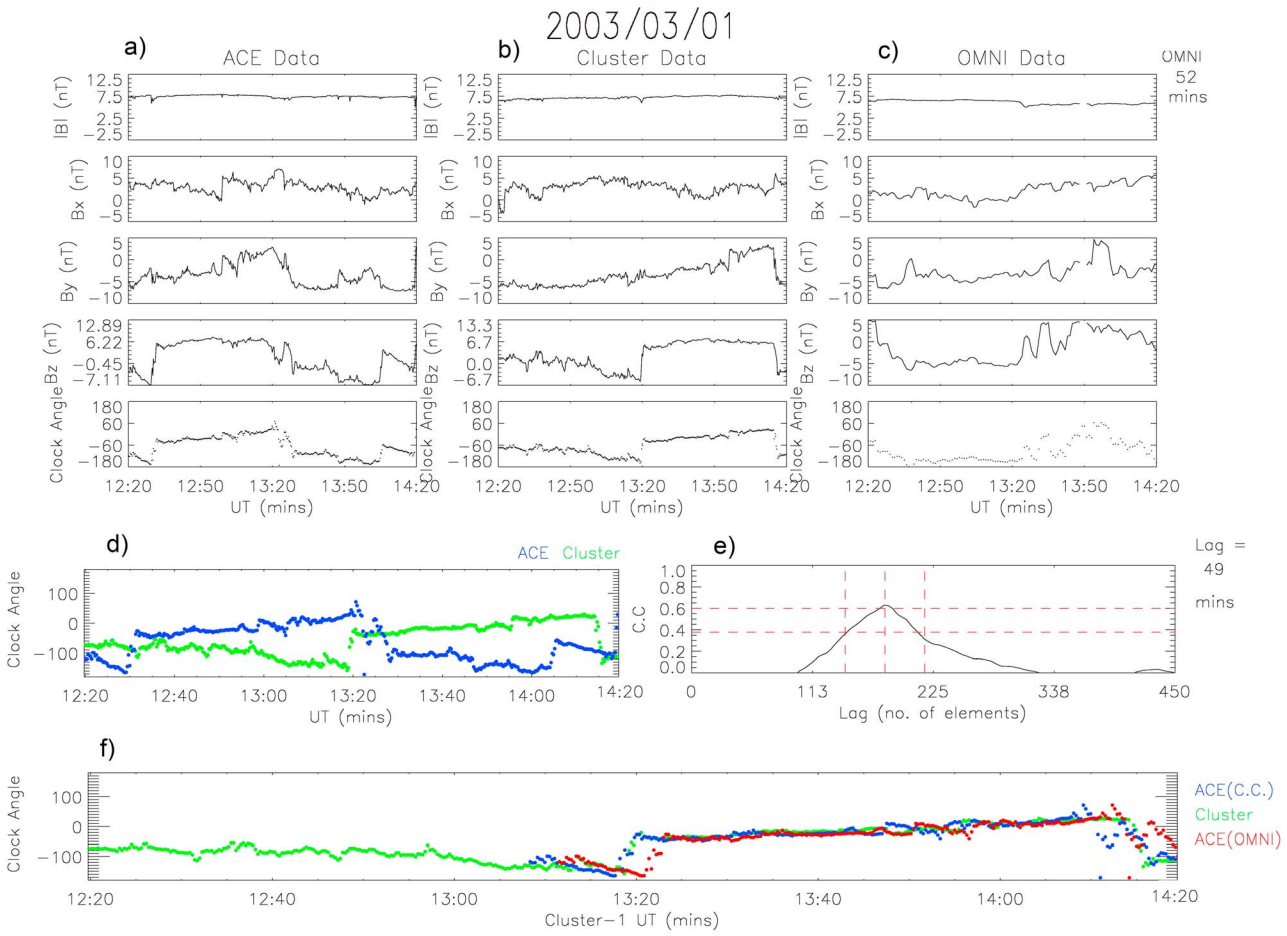

Figure 1. An example where all correlation conditions are met and the resultant delay would be included. (a and b) The magnetic field conditions at ACE and Cluster; (c) the corresponding OMNI data. (d) The clock angle at ACE (blue) and at Cluster (green) on the same time series. (e) The cross-correlation profile with the horizontal red lines indicating the maximum threshold (0.4) and the minimum correlation (0.6); the vertical lines indicate the 10 min window about the highest peak. (f) The clock angle at ACE lagged by the calculated cross-correlation delay in blue and by the OMNI delay in red. Shown in green is the measured clock angle at Cluster.

at a finite velocity over a finite distance; it is therefore not unreasonable to set the minimum condition at 0 min. If it is assumed that the propagation delay between the spacecraft is typically 1 hour, a maximum limit of 2 hours is reasonable.

2.2. Quality Measures

[21] To ensure that the delays calculated by the cross-correlation function were valid, several quality measures were introduced on the resultant correlation profiles. One of these conditions was applied to all data, while two further conditions were variable and could be adjusted to view their effects on the quantity and quality of data.

[22] The compulsory condition was that the peak of the correlation function must be positive. A negative correlation would imply that the data is anti-correlated which is unphysical in this case.

[23] The first of the two variable quality measures was the minimum acceptable correlation coefficient. By defining a minimum correlation coefficient, only those delays calculated from data which correlates at this minimum level or higher are included. If this level is set high, then only data which has correlated well is used and so the confidence in the quality of the calculated delay is increased. However, if this level is set too high then significant amounts of data would no longer meet the criteria and would be excluded from the results.

[24] The correlation function will often produce several peaks; sometimes it is clear which peak is more dominant from visual inspection, however in other cases there may only be a slight difference in the height of the peaks. In order to confidently determine the propagation delay, the correlation coefficient peak (i.e. a delay at which the correlation coefficient is at its highest) must be distinct. The definition of distinct is somewhat arbitrary, thus requiring the use of the second variable condition. The maximum threshold condition ensures that any secondary peaks are not more than a set percentage of the largest correlation coefficient peak, e.g. a 0.4 threshold condition ensures that any secondary peaks are less than 40% of the primary peak.

[25] In addition to the correlation function, a least squares fit was performed on the data sets for different delay values. Only if the least squares minimum coincided with the

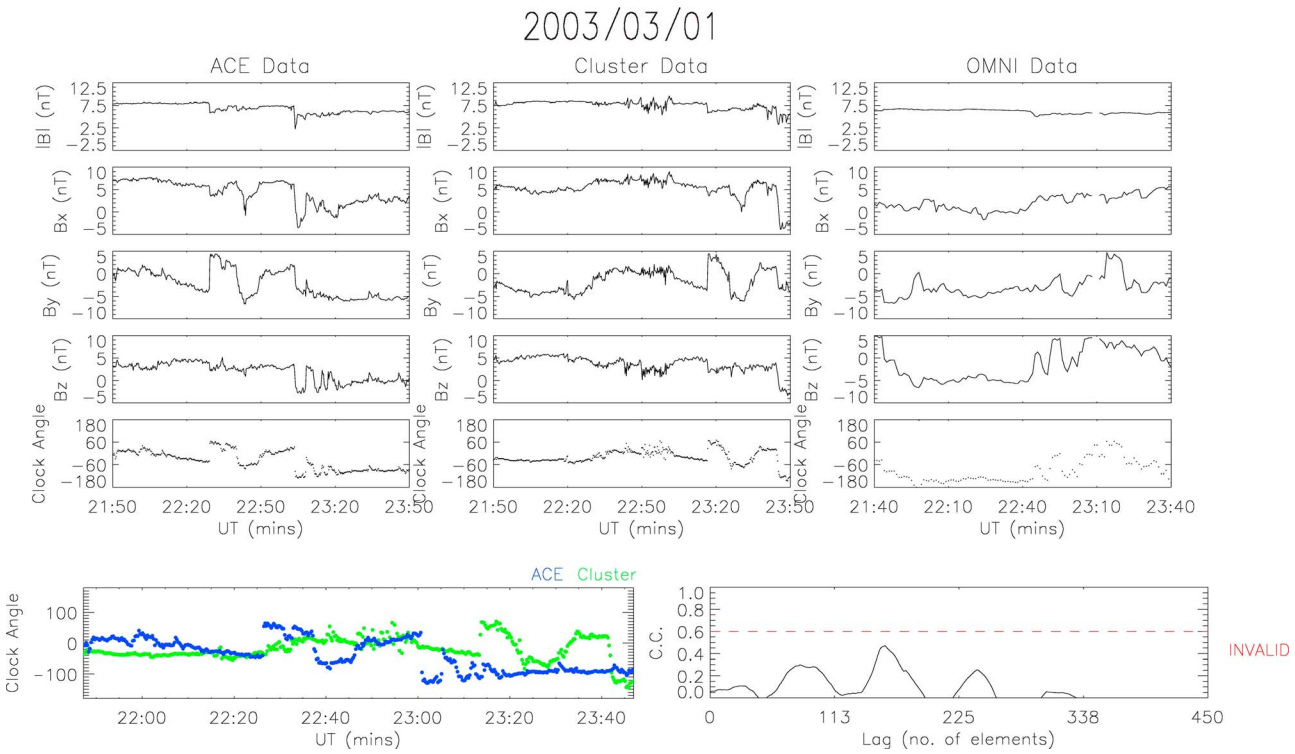

Figure 2. An example where the correlation conditions are not met, specifically the maximum correlation coefficient fails to meet the required minimum level; therefore the delay is not accepted. The format of the figure is the same as Figure 1.

maximum correlation peak was the delay recorded. This was to ensure that not only did the two data sets correlate but that they also aligned.

[26] Figure 1 demonstrates the methodology of this study. The top 15 plots, in Figures 1a–1c, show the IMF conditions between 12:20 and 14:20 UT at ACE and Cluster-1 and the corresponding OMNI data for the same UT interval. Figure 1d shows the clock angle at ACE in blue and at Cluster in green. Clearly, the clock angles do not match up due to the solar wind propagation delay from ACE to Cluster.

[27] Figure 1e is of the cross-correlation profile, showing the corresponding correlation coefficients as a function of the number of elements the segment of ACE data is shifted by. Finally, if the correlation conditions are met, the full width plot, Figure 1f, shows the clock angle measured by ACE shifted by the calculated propagation delay in blue, shifted by the corresponding averaged propagation delay from OMNI in red and the clock angle measured at that time at Cluster in green. In this example, when the clock angle measured by ACE is shifted by the cross-correlation delay it clearly aligns with the Cluster clock angle (which is expected) and it also aligns much more closely than when it is shifted by the OMNI delay.

[28] Figure 1 is an example where the cross-correlation meets all required conditions and, as such, the delay it produces would be accepted. There is clearly only one distinct peak in its correlation profile, in addition, this peak is positive and of a value which meets or exceeds the minimum correlation value.

[29] Of course, this is not always the case and depending upon the conditions set in place, much of the data may be rejected. Figure 2 displays the data in the same format as in Figure 1, for a different time period in March 2003; however, the computed delay is not accepted because the maximum correlation peak in Figure 2 fails to meet the required minimum correlation coefficient. In addition, while there is a larger peak in the correlation, there are also multiple smaller peaks indicating that this example may fail on the threshold condition also.

3. Results

[30] In the following section, the cross-correlation delays are compared against those predicted by the OMNI data set. OMNI freely provide high resolution solar wind data, such as the solar wind plasma and IMF parameters, which have already been lagged to the bow shock nose. Since this lagging is a non-trivial process, the OMNI data set is a widely used and accepted source of solar wind data.

[31] The OMNI team have accounted for several different variables when they produced their estimated propagation times, as shown in equation (1), though to achieve such high resolution data two key assumptions are made. First, the solar wind travels in a series of phase fronts, but any curvature in these fronts is ignored, and secondly that these fronts convect at the solar wind velocity.

[32] With the amount of data available in this study it is possible to directly test the OMNI model in a statistical survey, not just as a specific case study. This study will also

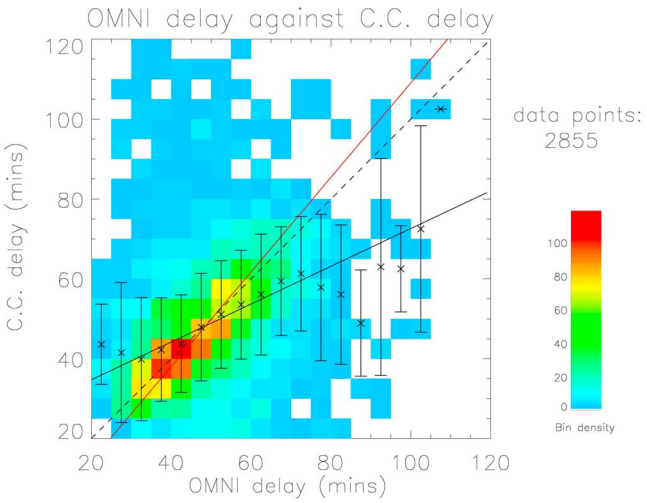

Figure 3. A density plot of the OMNI delay against the cross-correlation delay. There are no quality constraints in place on the data. The black line is a standard least squares fit, while the red line is least squares fit which incorporates the standard deviation of data.

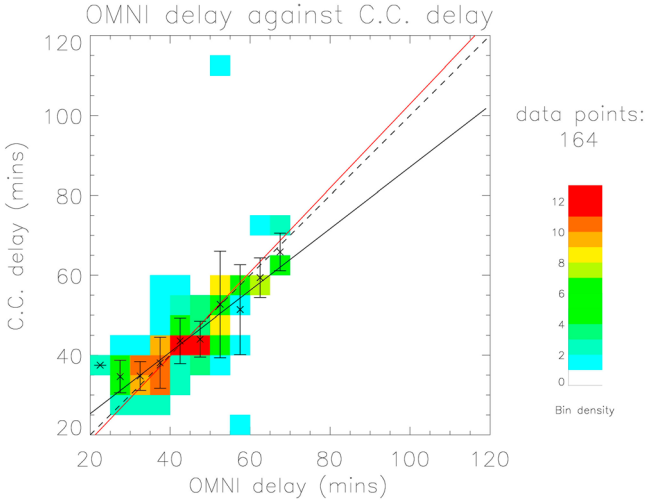

Figure 4. A density plot of the OMNI and cross-correlation delays constrained by a minimum correlation of 0.6 and maximum threshold of 0.4.

show the relationship of two delays based upon the solar wind speed and IMF orientation, as measured by ACE.

[33] Plotted in Figure 3 are the corresponding OMNI and calculated cross-correlation delays. They have been grouped into 5 min bins and their density is represented using the color scale. The cross in each column denotes the mean average for that column; the "error" bars represent ±1 standard deviation from the mean.

[34] The origin of the plot has been set at 20 min on both axes, rather than zero, since it was found that the minimum flat delay was 23 min, with the overwhelming majority of flat delays greater than 30 min. It was therefore considered unlikely that any cross-correlation delay or OMNI delay was correct if it was estimated to be less than 20 min.

[35] The data shown in Figure 3 have no quality measures in place (i.e. no restrictions on the minimum correlation or maximum threshold), resulting in 4938 delays produced from the 2001–2010 Cluster data set.

[36] The black line in the plots is a standard least squares fit computed from all data points; while the red line is a modified least squares fit, again computed from all data points, which also incorporates the standard deviation of the two data series. This modified least squares function is able to reduce the effect of an outlying point when calculating the line of best fit.

[37] There is considerable spread in the delays shown in Figure 3, however, note that the blue colored bins are an order of magnitude less in density than the red colored bins. The plot clearly exhibits a dense grouping of delays in the region of 30–60 min (on both axes). The averages of the columns in this dense grouping all fall, within ±1 s.d., on the $y = x$ line.

[38] In Figure 4, the OMNI and cross–correlation delays are again compared, in the same format as before. However, the quality constraints of minimum correlation coefficient 0.6 and maximum threshold 0.4 now in place, resulting in 164 delays plotted.

[39] Most of the spread has been filtered out, with just one outlier significantly off the $y = x$ line, and almost all of the column averages lie within ±1 s.d. from the $y = x$ line. Only the high density region observed in Figure 3, corresponding to delays of approximately 30–70 min, remains.

3.1. A Flat Delay

[40] Figure 5 presents the density of delays for the cross-correlation delay against the flat delay, using the same format as in Figure 3. It is quite apparent that the cross-correlation method can produce delays which are much longer than their equivalent flat delay. However, as with Figure 3, there is a clear high density grouping from around 30–60 min which seems to fit well with the y = x line.

[41] Figure 6 shows the density of delays from the OMNI data set against the flat delay with the same formatting as the earlier density plots. The delays used here are from the

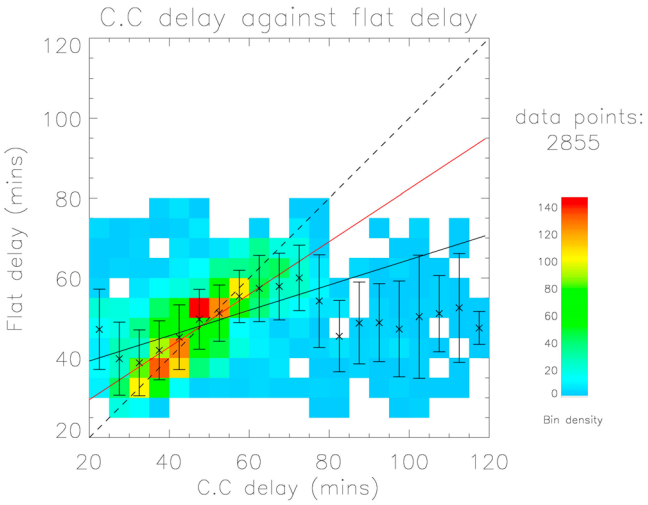

Figure 5. A density plot of the cross-correlation delay against flat delay.

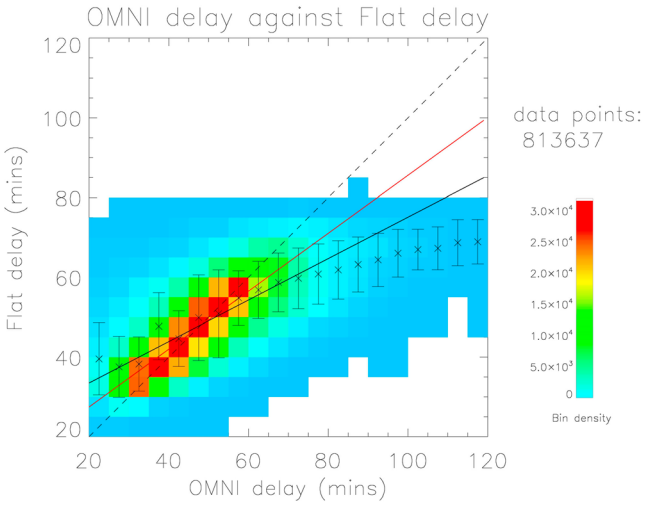

Figure 6. A density plot of the OMNI delay against the flat delay.

months where Cluster's orbit would primarily pass outside of the bow shock, i.e. January–April, for seasons 2001 through 2010. The delays are not limited to those matching up with the delays calculated by the cross correlation method. There is considerably less spread than with the cross-correlation plots and, as with the other plots, there is a high density region from approximately 30–60 min (on both axes) which fits well with the $y = x$ line. Note how the red colored bins are four orders of magnitude greater than the blue colored bins.

3.2. The Effect of Solar Wind Speed

[42] Solar wind speed is defined herein as the x-component of the solar wind velocity, as the solar wind flows past ACE, averaged over the cross-correlation period.

[43] In Figure 7, the OMNI and cross-correlation delays are compared and colored by the solar wind speed. As in Figure 4 the data are constrained by a minimum correlation coefficient of 0.6 and maximum threshold of 0.4.

[44] In order to determine what effect, if any, the solar wind speed may have on the relationship between OMNI and the cross-correlation delay method, it is prudent to split the delays depending upon their respective solar wind speed. In Figure 7 the delays have been grouped into slow, medium and fast solar wind speeds. Rather than arbitrarily choosing what limits each grouping should have, the groupings were determined using tertiles.

[45] As would be expected, there is a general trend indicating that slower solar wind speeds tend to produce longer

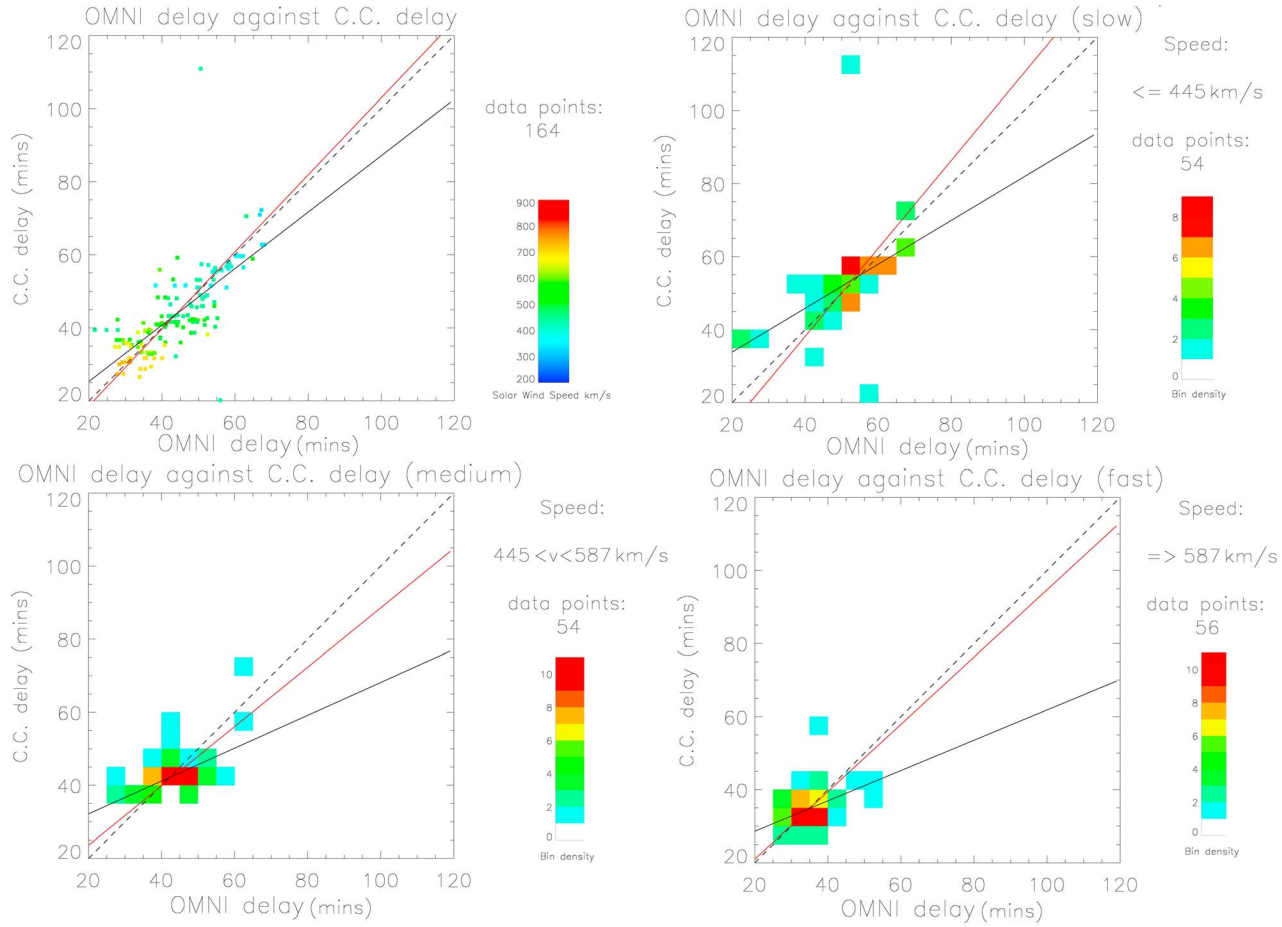

Figure 7. OMNI and cross-correlation delays are represented by their respective solar wind speed. In the first of the plots in the figure, the delays are colored by their speed. In the three other plots, the delays have been split into slow, medium and fast speeds and shown as density plots.

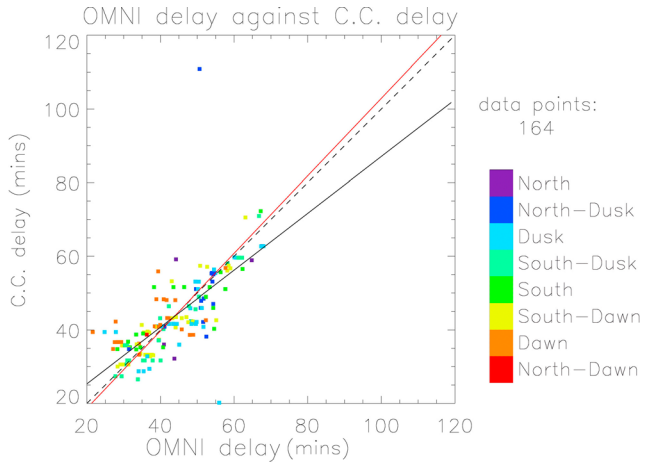

Figure 8. A scatterplot of the OMNI and cross-correlation delay represented by solar wind clock angle.

delay times than the faster solar wind. There is good agreement between OMNI and the cross-correlation method for fast, medium and slow solar wind speeds when using the modified least squares fit function. However, when using the standard least squares fit function the agreement seems to worsen as the solar wind speed increases.

3.3. The Effect of IMF Orientation

[46] The orientation of the IMF can be described using spherical coordinates, where the inclination and azimuth angles are the clock angle and cone angle respectively.

[47] The clock angle may be calculated as previously shown in equation (2); while the cone angle, as shown in equation (4), is the arctangent of the x-component of the magnetic field over the magnitude of the y-and z-components of the magnetic field.

$$\phi = \arctan\left[\frac{Bx}{\sqrt{(By^2 + Bz^2)}}\right] \tag{4}$$

[48] The following figures show the OMNI and cross-correlation delays colored by their clock angle in Figures 8 and 9 and by their cone angle in Figure 10.

3.3.1. Clock Angle

[49] The clock angle has a range of 360 degrees. A vector with clock angle 0°/360° points in the upward direction perpendicular to the plane of the Earth's orbit, hereafter referred to as "North," and with 180° points downward, hereafter referred to as "South"; vectors with clock angles of 90° and 270° point Duskward and Dawnward respectively.

[50] Figure 8 shows the delays by the different clock angles for minimum correlation coefficient 0.6 and maximum threshold 0.4. Since the clock angle freely fluctuated during the correlation periods, the clock angles were binned into 45° sectors and the most common sector value was chosen as the clock angle for that period.

[51] The sectors of 45° were specifically chosen so as to be aligned with the major and semi-major orientations and the densities of these sectors are shown in Figure 9. This will indicate what, if any, statistical effect the direction of the solar wind has upon the relationship between the OMNI and cross-correlation delays.

3.3.2. Cone Angle

[52] The cone angle has a range of 180° (±90°); a vector with a−90° cone angle points toward the Earth along the Earth-Sun line while one with a+90° cone angle points toward the Sun. Figure 10 shows the directionality of the IMF, by its cone angle, for a minimum correlation coefficient of 0.6 and a maximum threshold of 0.4. As with the clock angle, the cone angle chosen for the correlation period was the most common sector value. However, in the case of the cone angle three specific sectors were chosen: angles primarily pointing in the positive GSE x-direction; in the negative GSE x-direction and in the direction of the z-axis.

[53] In the first plot in the figure, the delays have been colored by their sector cone angle. The other three plots in the figure show the density of delays for each sector.

4. Discussion

[54] We have presented a statistical analysis of nearly 5000 solar wind propagation delays, reduced to 164 delays after quality filtering, calculated by performing a cross-correlation function on magnetic field data from ACE and Cluster-1. We required that Cluster was upstream of the bow shock at 15 R_E from Earth (in the GSE x-direction) and that the on-board CIS instrument recorded ion temperatures of below 1 keV. Two further quality conditions filtered out those delays whose correlation profiles were deemed to be of poor quality and a least squares fit condition ensured that the resultant clock angle data mapped each other well.

[55] Manual inspection of the data, and their resultant correlation profiles, found that the cross-correlation analysis worked best, i.e. provided distinct and substantial correlation peaks, when there was a distinct discontinuity in the IMF clock angle. Other studies, such as *Mailyan et al.* [2008], had primarily only considered such cases, though those events were chosen through manual filtering, resulting in far fewer delays calculated. However, once our quality conditions were in place, our data set was subsequently reduced to a similar size as used by *Mailyan et al.* [2008].

[56] We have shown how altering the two quality conditions can severely impact upon the amount of usable data. With no conditions in place there were 4938 calculated propagation delays, but when the quality controls were set at minimum correlation 0.6 and maximum threshold 0.4 the usable data was diminished to 164 delays. Altering the minimum correlation had the greatest effect on the reduction in usable data by far, most likely because as the correlation of the peak increases the likelihood that it is a distinct peak should increase (if the time series is not periodic). There is, therefore, a trade-off between having a large data set and having a high quality data set.

[57] *Crooker et al.* [1982] had previously applied the cross-correlation method to IMF measurements between ISEE 1 and ISEE 3. They determined that a coherence scale length of 90 R_E existed for magnetic structures embedded within the solar wind and that for separation distances greater than this scale length the quality of the correlation decreases substantially. Their findings agree well with other studies such as *Chang and Nishida* [1973] and *Sari and Valley* [1976], who also found coherence scales with a maximum length of 80 R_E and 150 R_E respectively. The separation distance between ACE and Cluster (~225 R_E) is

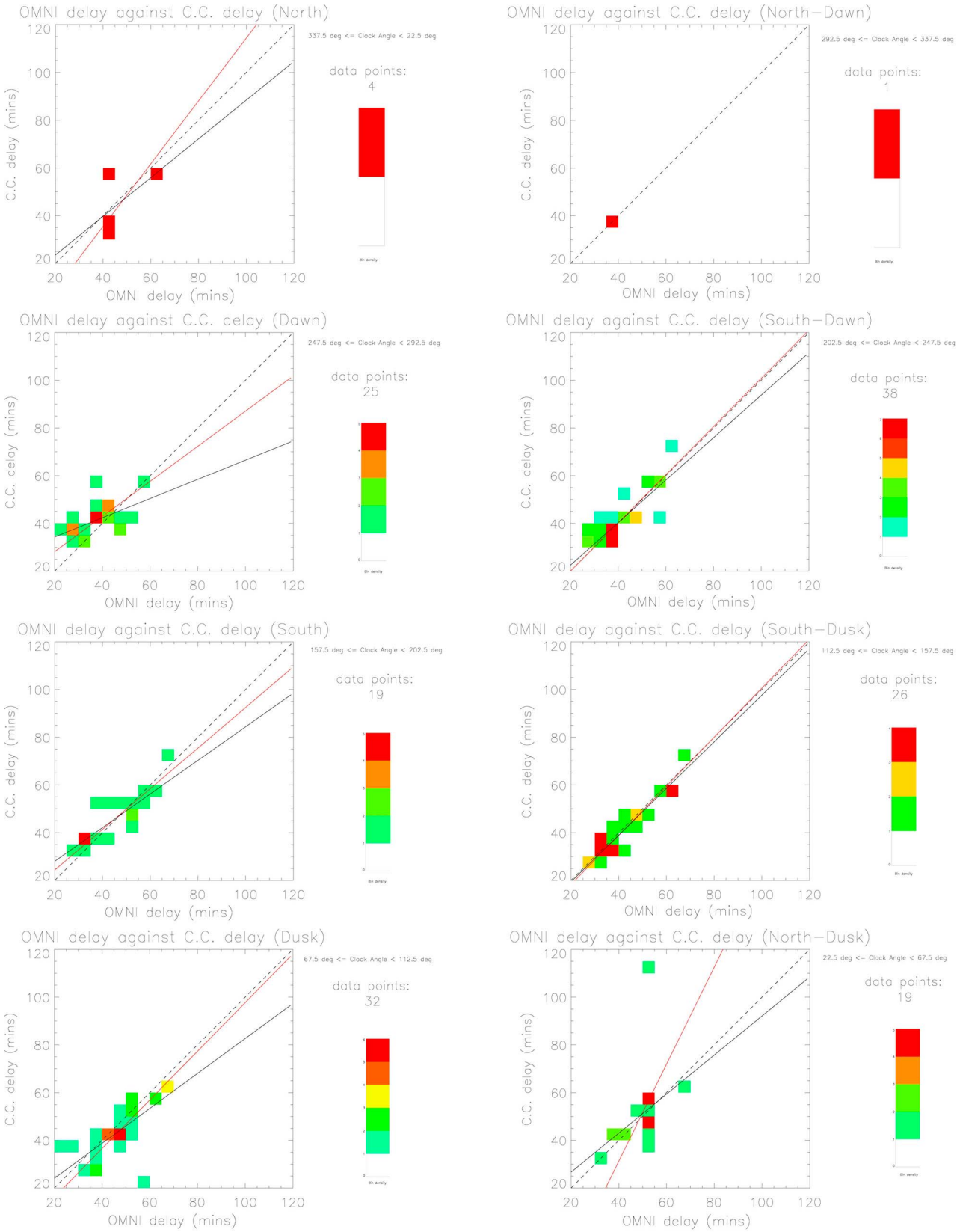

Figure 9. Delays represented by clock angle, grouped into eight directions. The quality conditions imposed were minimum correlation 0.6 and maximum threshold 0.4.

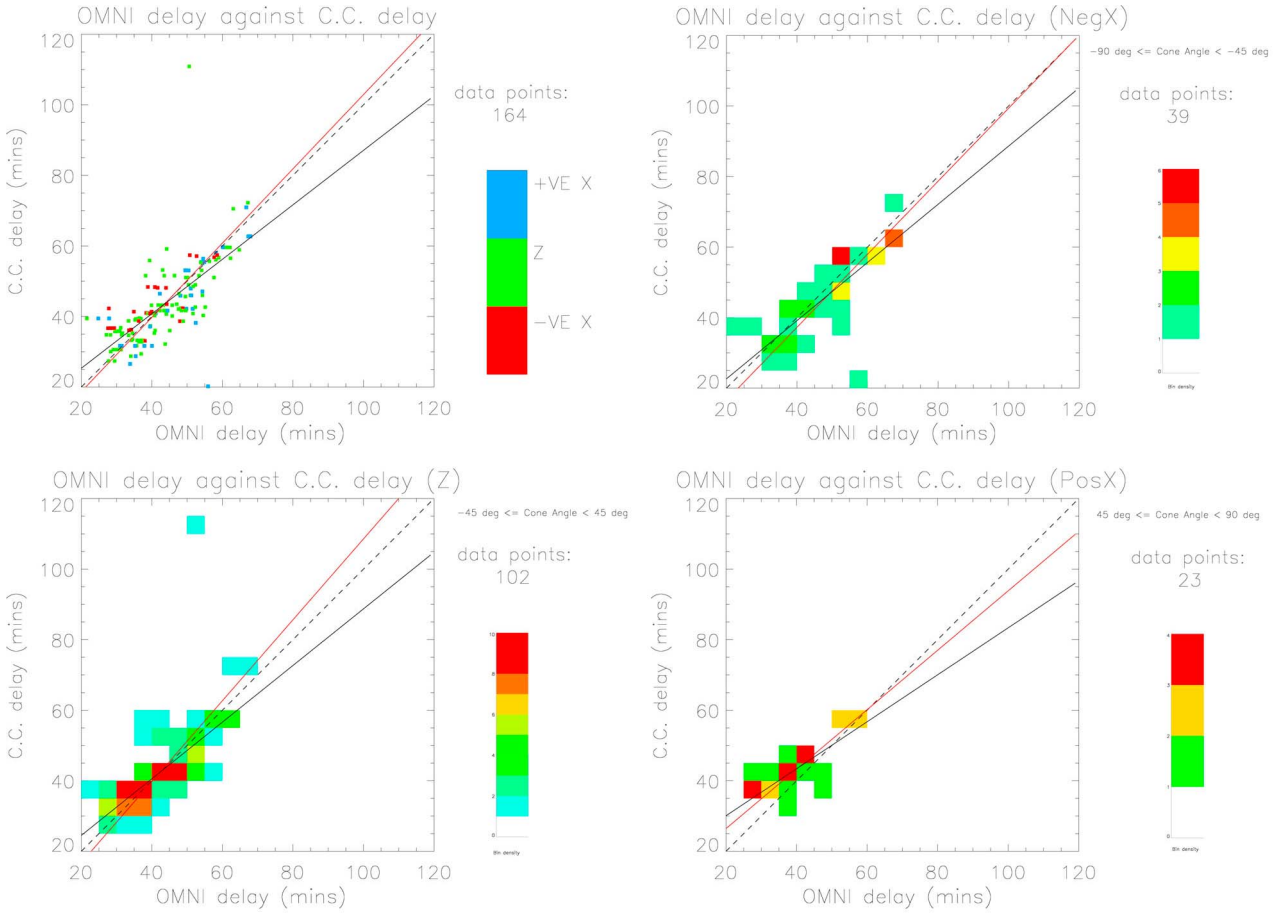

Figure 10. Delays represented by the decomposed solar wind cone angles.

far greater than any of those coherence scale lengths and so it is unsurprising that such a reduced number of delays is noticed at high correlation requirements.

[58] In Figure 3, OMNI's 10 min-averaged delay times were directly compared to the cross-correlation delay times, with no quality conditions in place, in the form of a density plot. There is considerable spread, especially at longer cross-correlation delays but correspondingly short OMNI delays. However, the densities of these bins is very low and in most cases is less than ten delays per bin. Two possible scenarios exist to explain this: either OMNI underestimates those delays or the cross-correlation method has overestimated them.

[59] A modified least squares fit (shown as red on the plot) has a gradient of 1.18 ± 0.024 and intercept of -9.23 ± 0.05, while this may indicate an 18% difference in the gradient when compared to the $y = x$ line, owing to the intercept it only amounts to a maximum difference of the order of a couple of minutes from the $y = x$ line in the high density region. The distribution of the column means further indicate that the two methods agree particularly well in the very high density region (approximately 30–70 min) where all the means fit within 1 s.d. of the $y = x$ line. The relationship does not hold as well at longer OMNI delay times (>80 min) since the column averages of the cross-correlation method do not increase.

[60] When the quality constraints of minimum correlation coefficient 0.6 and maximum threshold of 0.4 are in place, as in Figure 4, the number of data points is reduced significantly and so too is the amount of spread in the data. Nearly all the column means are within 1 s.d. of the $y = x$ line and the modified least squares fit is described by $y = (1.05 \pm 0.24)x - (2.39 \pm 0.14)$. There is no extended delay (>80 min) region for either methods.

[61] The flat delays are compared to the cross-correlation delays in Figure 5. Again, the spread is considerable, especially at longer delays. The modified least squares fit gradient (red) is 0.66 ± 0.12 with an intercept of 16.3 ± 0.03, indicating that the cross-correlation method, in general, predicts longer delay times, especially in the extended delay region. It could be that the flat delay underestimates the delay or that the cross-correlation function, in some case, overestimates it.

[62] In Figure 6, the OMNI 1-min resolution delays are compared to the calculated flat delays. The gradient of the modified least squares fit (red) is 0.73 ± 0.06 with an intercept of 12.95 ± 0.00 and the column means in the high density regions fit within 1 s.d. so, as with the previous two plots, the two sets of delays seem to agree well, with OMNI having a slight tendency to produce longer delays than the flat model in the extended delay region.

[63] Since both OMNI and the cross-correlation method tend to estimate longer delay times than the flat model, it seems likely that the flat model underestimates the delay time (rather than the other two methods overestimating it) in the extended delay region. The flat model rarely predicts a

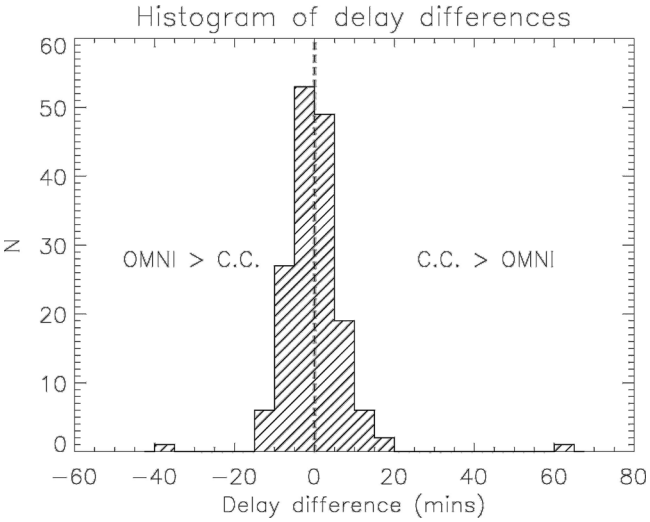

Figure 11. A histogram of the differences between the OMNI and cross-correlation delays.

delay which is longer than 80 min; whereas both OMNI and the cross-correlation method do so much more frequently.

[64] The OMNI and the cross-correlation delays were then compared based upon the solar wind speed in Figure 7. There seems to be no effect on the relationship between the two methods based upon the speed of the solar wind. The lines of best fit in the fast solar wind have tilted away from the $y = x$ line, with a gradient of less than one, however, this is due to the "turning power" of an outlying point, rather than a real trend.

[65] Figure 9 presents the OMNI and cross-correlation delays by clock angle in eight separate plots. The IMF clock angle dawn-dusk preference, a result of the Parker spiral, is clearly demonstrated in the density plots, with a distinct lack of delays for northward pointing clock angles. With the exception of the north-dawnward (for lack of data) and the north-duskward pointing clock angles, there is no significant difference between the relationship of the OMNI delays and the cross-correlation delays for different clock angles. The north-duskward clock angle plot shows a large spread in delays but there is no determinable reason known to us as why this spread should occur and may simply be a statistical anomaly.

[66] The cross-correlation and OMNI delays, sorted by IMF cone angle, are presented in Figure 10. The cones angles are split into three directions: primarily pointing in the positive and negative GSE x-directions and primarily pointing in the positive GSE z-direction. There is little difference between the three directions, suggesting that the IMF cone angle has no effect on the relationship between the two delay methods.

5. Conclusions

[67] Our study has shown that statistically there is little difference in the delays calculated by OMNI, the cross-correlation method and the flat propagation model, however, there is often considerable spread in the compared delays. This indicates that, in general, the methods agree well; but, on occasion, the methods can produce delays which differ by over 30 min.

[68] In Figure 11 the differences between the OMNI and cross-correlation delays are shown. The histogram shows that the vast majority of delays differ by less than 15 min, with two instances where the delays differ by over 30 min.

[69] The cross-correlation method uses data from ACE and Cluster to calculate its delay times directly, rather than through use of a model, and so is independent of many assumptions required when using a model, though some assumptions are needed, e.g. that the signal is effectively the same at both spacecraft and has simply propagated between them. If the cross-correlation method were flawless, it should be a true representation of the propagation delay, and if the OMNI delays were accurately calculated then it is logical to assume that they should, statistically at least, present very similar results to that of the cross-correlation method.

[70] Interestingly, the flat propagation model produces very similar results also, especially for delays $\leq$80 min. However, there is an extended delay region (or a "tail"), when compared with the other two delay methods, for delays >80 min, indicating that the flat propagation model is too simple and fails to account for times of longer delay. Several studies have shown that delay times are affected by tilted IMF variations [e.g., *Weimer et al.*, 2003] and the tail could be the physical representation of this.

[71] Of course, the cross-correlation method is not a definitive calculation for the delay time. Several factors affect the reliability of this method, most notably the separation distance between the first and second observers; which, in the case of ACE and Cluster, is a significant separation and one which, according to *Crooker et al.* [1982], is far greater than the correlation coherence length of the solar wind structures.

[72] It is also noted that the distance not only in the GSE x-direction, but also in the y-direction may have a significant affect on the delays calculated as in this study no limits were set on the distance of Cluster, or ACE, from the Earth-Sun line. However, *Richardson et al.* [1998] had previously shown that correlation coefficients between ISEE 3 (at L1) and IMP 8 (in a circular orbit about the Earth) had little dependence upon the separation of the craft in the y-direction since the separation distance in the x-direction was much greater. In our periods of interest, Cluster's maximum deviation from the Earth-Sun line, in the y-direction, was $\pm 10\ R_E$ while ACE's maximum deviation was $\pm 40\ R_E$ whereas their separation in the x-direction was 225 R_E. It was therefore assumed that these deviations from the Earth-Sun line would not have the same impact as the x-direction separation distance.

[73] The relationship between the cross-correlation and OMNI delays, at minimum correlation 0.6 and maximum threshold 0.4, is not affected by the orientation of the IMF; except, perhaps, for the North-Duskward clock angle where a greater spread was noticed; nor is it particularly affected by the solar wind speed. This would seem to indicate that, since OMNI accounts for the IMF orientation in its estimations, via the PFN, and that we see no obvious difference with the cross-correlation, the PFN does indeed affect the delay time.

[74] Unlike other techniques, the cross-correlation method does not require a discrete discontinuity in the IMF to

calculate a delay time. However, clearly, for occasions where such discontinuities exist the cross-correlation delay is more likely to be representative of the true propagation delay, than for those occasions where the clock angle is almost constant ("flat"). Note that if the clock angle were indeed truly flat throughout the cross-correlation period, there would be perfect correlation for every delay time, which would be meaningless in this context.

[75] The findings of this study can be summarized as follows:

[76] 1. The cross-correlation analysis provides a method to benchmark the propagation delays of the solar wind as it traverses from L1 to Cluster in the vicinity of the bow shock nose, as predicted by the OMNIweb service. Although the cross-correlation method does not rely on distinct discontinuities in the solar wind, it is likely to produce higher quality estimates when they are present.

[77] 2. When no quality controls on the correlation were in place, nearly 5000 delays were calculated from 10 years of ACE and Cluster data. However, when the data were constrained to reject ambiguous correlations, this amount diminished significantly to 164 delays.

[78] 3. With the constrained data, the OMNI and cross-correlation methods gave statistically similar results. However, we note that individual delays derived from the OMNI and cross-correlation techniques delays could differ by up to 50%.

[79] 4. Although equivalent delays computed by the two techniques can differ substantially, examination of prevailing upstream parameters revealed no solar wind/IMF control over the cross-correlation-OMNI relationship.

[80] 5. Based on these findings, we suggest that to determine the solar wind conditions during a period of interest, it is preferable to employ the use of a solar wind monitor just upstream of Earth at the bow shock. However, we acknowledge that this is not always possible and that the OMNIweb data products are convenient and provide statistically valid upstream parameters.

[81] **Acknowledgments.** We gratefully acknowledge the NASA/GSFC Space Physics Data Facility's OMNIWeb service. For details of OMNI's calculations, visit http://omniweb.gsfc.nasa.gov/html/sc_merge_data1.html. We also acknowledge ACE and CDAWeb for the magnetic solar wind data, and we would like to acknowledge the Cluster Active Archive data facility and the Cluster FGM and CIS teams for the use of the Cluster data. N. C. is supported by an STFC studentship.

[82] Robert Lysak thanks the reviewers for their assistance in evaluating this paper.

References

Chang, S. C., and A. Nishida (1973), Spatial structure of transverse oscillations in the interplanetary magnetic field, *Astrophys. Space Sci.*, *23*, 301–314.

Crooker, N. U., G. L. Siscoe, C. T. Russell, and E. J. Smith (1982), Factors controlling degree of correlation between ISEE 1 and ISEE 3 interplanetary magnetic field measurements, *J. Geophys. Res.*, *87*, 2224–2230.

Farris, M. H., and C. T. Russell (1994), Determining the standoff distance of the bow shock: Mach number dependence and use of models, *J. Geophys. Res.*, *99*, 17,681–17,689.

Horbury, T. S., D. Burgess, M. Franz, and C. J. Owen (2001), Prediction of Earth arrival times of interplanetry southward magnetic field turnings, *J. Geophys. Res.*, *106*, 30,001–30,009.

Mailyan, B., C. Munteanu, and S. Haaland (2008), What is the best method to calculate the solar wind propagation delay?, *Ann. Geophys.*, *26*, 2383–2394.

Richardson, J. D., F. Dashevskiy, and K. I. Paularena (1998), Solar wind plasma correlations between L1 and Earth, *J. Geophys. Res.*, *103*, 14,619–14,629.

Sari, J. G., and G. C. Valley (1976), Interplanetary magnetic field power spectra: Mean field radial or perpendicular to radial, *J. Geophys. Res.*, *81*, 5489–5499.

Shue, J. H., J. K. Chao, H. C. Fu, C. T. Russell, P. Song, K. K. Khurana, and H. J. Singer (1997), A new functional form to study the solar wind control of the magnetopause size and shape, *J. Geophys. Res.*, *102*, 9497–9511.

Stone, E. C., A. M. Frandsen, R. A. Mewaldt, E. R. Christian, D. Margolies, J. F. Ormes, and F. Snow (1998), The Advanced Composition Explorer, *Space Sci. Rev.*, *86*, 1–22, doi:10.1023/A:1005082526237.

Weimer, D. R., and J. H. King (2008), Improved calculations of interplanetry magnetic field phase front angles and propagation time delays, *J. Geophys. Res.*, *113*, A01105, doi:10.1029/2007JA012452.

Weimer, D. R., D. M. Ober, N. C. Maynard, M. R. Collier, D. J. McComas, N. F. Ness, C. W. Smith, and J. Waterman (2003), Predicting interplanetary magnetic field (IMF) propagation delay times using the minimum variance technique, *J. Geophys. Res.*, *108*(A1), 1026, doi:10.1029/2002JA009405.

N. A. Case and J. A. Wild, Department of Physics, Lancaster University, Lancaster LA1 4YB, UK. (n.case@lancaster.ac.uk)